

ICANS-VI  
INTERNATIONAL COLLABORATION ON ADVANCED NEUTRON SOURCES  
June 27 - July 2, 1982

MEASUREMENTS OF THE SPALLATION AND FISSION PRODUCT  
PRODUCTION FOR DEPLETED URANIUM AND NATURAL LEAD  
TARGETS BOMBARDED BY 1100 MEV PROTONS

W. Amian, N.F. Peek\*, D.J. Shadoan\*

Institut für Reaktorentwicklung  
Kernforschungsanlage Jülich GmbH  
Postfach 1913  
D-5170 Jülich 1, Germany

\*Physics Department, University of California,  
Davis, California 95616

ABSTRACT

In order to simulate the spallation source target, 3 cm diameter by 1 mm thick disks of natural lead and depleted uranium were irradiated at 1100 MeV proton energy. The targets were inbedded between 5 cm thick bricks of the respective material. Gamma-ray spectrometric methods of gamma-peak and halflife analysis were developed to deduce mass yield distributions of the radionuclides produced. Both for lead and uranium fission products have been observed. The mass yield distributions and axial distributions of some isotopes are given. For lead the total production rates of some isotopes within an 100 x 50 x 450 mm target block are given.

MEASUREMENTS OF THE SPALLATION AND FISSION PRODUCT  
PRODUCTION FOR DEPLETED URANIUM AND NATURAL LEAD  
TARGETS BOMBARDED BY 1100 MEV PROTONS

W. Amian, N.F. Peek\*, D.J. Shadoan\*

Institut für Reaktorentwicklung  
Kernforschungsanlage Jülich GmbH  
Postfach 1913  
D-5170 Jülich 1, Germany

\*Physics Department, University of California,  
Davis, California 95616

#### INTRODUCTION

Development of a high flux neutron source utilizing the spallation reaction necessarily involves extensive study of residual activity produced in the target material. To accommodate this task, gamma-ray spectrometric methods have been developed to deduce mass yield distributions for proton-induced spallation and fission reactions.

Measurements have been performed for thick targets of depleted uranium and natural lead bombarded by 1100 MeV protons. The axial distributions of the spallation and fission products observed within an 1.5 cm radial interval around the beam axis have been measured. Some of these results are given in this paper. For the uranium target especially the depth dependent production of Pu 239 by its precursor Np 239, the production of U 237 and of the fission product Ru 103 are given.

Preliminary mass yield distributions have been evaluated for 1 mm thick target foils exposed to the proton beam at the surface of the thick targets. Both for lead and uranium targets, fission products have been observed.

## EXPERIMENTAL PROCEDURE

The experimental procedures involved irradiation of relatively thin, 1.0 mm thick, target foils embedded at equally spaced intervals in a larger target whose physical dimensions were similar to those of the proposed "infinitely thick" spallation target wheel. Two target materials were chosen for investigation, natural Pb and depleted U. An 1100 MeV proton beam at Saturne National Laboratory within the Centre d'Etudes Nucleaires de Saclay with an average intensity of up to 80 nA was used for irradiations. Once irradiated the target foils were removed and counted using high resolution gamma-ray spectroscopy. The resulting data were recorded on magnetic tape for subsequent computer analysis and isotope identification /1/. Figure 1 shows the configuration of the Pb target in detail. The first target foil shown was an aluminium foil (3.0 cm diameter by 1.0 mm thick) positioned 5.0 cm in front of the main target assembly. In this position it was utilized to monitor the incoming proton intensity. The next target foil (the first Pb foil) was positioned directly in front of the main assembly to receive full beam energy. Immediately behind the first Pb foil followed a 1.0 mm thick aluminium plate used to monitor the beam distribution.

The three target elements described above, Al foil, Pb foil, and Al plate, constituted a repetitive unit and appeared a total of 10 times; each unit separated by a 5.0 cm thick Pb brick. Individual target foils consisted of 3.0 cm diameter by 1.0 mm thick natural Pb disks. These dimensions were chosen as a compromise between adequate counting intensity and corrections due to self-absorption and non point-source geometry. Due to space limitations in the target area the total length,

45 cm, of the complete Pb target assembly was short of the "infinite thickness", 65 cm, required to completely absorb 1100 MeV protons. Stopping-power calculations indicated an energy loss of 700 MeV in 45 cm of Pb.

The uranium target foil assembly was identical except for two instances. First, the entire target assembly was infinitely thick at an overall length of only 35 cm and therefore the number of uranium target foils irradiated was eight in one run and nine in the next. Secondly, the uranium foils were vacuum encapsulated in aluminum cases to prevent the escaping of radioactive gases.

The data collection system included high resolution gamma-ray analysis electronics in conjunction with a 80 cm<sup>3</sup> Ge(Li) detector and an automatic sample changer mounted on rails to vary the distance to the detector easily. The detector was enclosed in lead shielding, 10 cm thick. The background due to photons with energies less than 100 keV, such as lead x-rays were excluded from the spectra by a lower level discriminator. The detector was calibrated against IAEA and PTB standard reference sources with + 2 % accuracy. The cross sections used to determine the number of protons striking the target for the respective proton reactions on aluminium are given in table 1. These have been taken from a review paper of Cummings /2/.

#### DATA REDUCTION

The gamma-ray spectra are analyzed by the computer code AGAMEMNON /3/. All spectra are corrected especially for energy calibration drift. The halflife analysis and nuclide identification code YELLOW /4/ is then applied to the peakfit results.

YELLOW sorts the outputs of AGAMEMNON by energy and time, plots the calculated activity for each peak-energy group as a function of time and identifies the reaction products based on their half-lives and known gamma-ray transitions. Besides the activity-time plot the system prints a list of all candidates which fit the experimental points best. The resulting decay curves of the best candidates are drawn in the graph (Fig. 2). If the decay is of parent-daughter nature, this is taken into consideration. Any number of overlapping nuclides may be taken into account, experience, however, revealed that a maximum of three is sufficient (for parent daughter decay, six).

Finally the program outputs the complete list of candidate nuclides ordered by atomic number and mass number (Fig. 3). The number of nuclei produced as calculated by the half-life analysis is given for each of the isotope's gamma-ray transition lines. To accept a candidate nuclide the dominant gamma-ray transition lines have to fit the decay curves at the respective energy most probably and these results have to agree within the experimental errors stated for the number of nuclei. These errors include besides the statistical errors of counting the fitting errors of the peakfit and the error of the half-life analysis. For dominant lines this is typically no more than 5 %. The list of candidate isotopes is derived from the compilation of Erdtmann and Soyka /5/, however the list of parent nuclei had to be enlarged for our purposes. For targets the library is scanned from atomic number  $Z = 4$  (Be) up to  $Z = 84$  (Po), for uranium up to  $Z = 94$  (Pu).

All results given have been corrected for decay during irradiation and for gamma-ray attenuation in the sample.

## EXPERIMENTAL RESULTS

Figures 4 and 5 show the axial distributions of Pt-191, Os-185, Y-88, Pb-203 and Hg-203 within 1,5 cm radial interval around beam axis.

The total number of reactions per proton within the target can be estimated by these data and by the measurements of the beam profile performed by looking at the Na-24 distribution on the aluminium plates inserted into the target. Table 2 gives the mean and FWHM of the vertical Gaussian beam profile, the Na-24 intensity and the fraction of the beam hitting the 3 cm-diameter target. The value of 15 % at a depth of 45 cm is near to a homogeneous activation of 14.1 % (target area/total area). The results of these calculations are given in table 3.

Figure 6 shows the number of reactions per proton and per ( $\text{g}/\text{cm}^2$ ) for a lead foil at the front target face for various mass numbers. A distinction has been made between de-excitations from proton rich ( $\beta^+$ ,  $\epsilon$ ) and neutron rich ( $\beta^-$ ) states, respectively. Starting from the mass of the heaviest lead isotope (208) the production of radioactive proton rich isobars increases sharply to a mass number at 200 (stable isotopes may be produced in addition) and drops off about two orders of magnitude to a mass number of 140. At masses  $< 110$  neutron rich fission products seem to be produced in competition with proton rich isobars.

The axial distribution of the fission product Rh-103, the Pu-239 precursor Np-239 and of the spallation product U-237 for the lead target bombarded at 1100 MeV proton energy are shown in figure 7. The distribution of Rh-103 is representa-

tive of the number of fissions and therefore for the energy deposition.

Figure 8 shows the number of reactions per proton and per ( $\text{g}/\text{cm}^2$ ) for a uranium foil at the front target face for various mass numbers. Again a distinction has been made between neutron rich and proton rich isobars. The neutron rich isobars at masses between 85 and 155 are the normal fission products. Their distribution has the expected shape. Proton rich isobars are produced in that region, too, but at a one order of magnitude lower rate. In the gap between mass numbers 160 and 190 no nuclides could be identified with certainty. The gap between mass number 210 and 230 is not accessible to  $\gamma$ -spectrometry, because the nuclides are short lived  $\alpha$ -emitters.\*

It can be assumed, that the fissions observed are mainly due to neutrons. This is shown in figure 9 where the axial distributions of the fission products Ba-140 and Nd-147 and of the proton rich product Xe-127 are compared to the results for a foil exposed to the proton beam 20 cm upstream from the target. While the production rates for the fission products drop off sharply, the one of Xe-127 remains nearly unchanged. This result however, should be taken qualitatively only, because the neutron flux in the upstream position is not known from experiment.

---

\*By integration of the distribution for neutron rich fission products using Simpson's Formula and relating it to 200 % yield an absolute yield of (5 + 2) % for mass 103 was estimated. Multiplying the numbers for Ru 103 in figure 9 by 20 gives the axial distribution of fission in the uranium target block in an 1.5 cm radial interval around beam axis.

## CONCLUSION

The experiments described in this study allow to measure the axial distributions within natural lead and depleted uranium targets for those spallation and fission products, which show dominant  $\gamma$ -ray lines. Because no chemical separations are done the gamma-ray spectra contain numerous overlapping peaks. The presence of a nuclide like Lu 170, having 596 known gamma-ray lines, in the spectra of the lead targets illustrates this fact. This is why the analysis of the spectra necessarily calls for extensive studies of the half-lives identifiable.

For both target materials preliminary mass yield distributions have been evaluated for 1 mm thick target foils exposed to the proton beam at the surface of the thick target blocks. Fission products have been observed in each case.

For uranium the shape of the fission product distribution for neutron rich isobars seems to imply the fission by low energy neutrons in competition to high energy particle processes. This is more substantiated by the fact, that a target foil irradiated 20 cm apart from the thick target shows a relatively higher decrease in the formation of neutron rich fission products as compared to proton rich fission products.

It is planned to compare our experimental data with calculated predictions using the Monte Carlo code HETC.



## REFERENCES

- /1/ N.F. Peek, D.J. Shadoan, W. Amian  
Gamma-ray measurements of isotopes produced  
by 1.1 GeV protons on lead and uranium targets  
ICANS-V, Jülich 1981
- /2/ J.B. Cumming  
Annual Review of Nuclear Science 13 (1963) 261
- /3/ W. Amian  
AGAMEMNON - a computer code to analyze complex  
gamma-ray spectra  
(in preparation)
- /4/ W. Amian, N.F. Peek, D.J. Shadoan  
Gamma-ray spectrometric product identification  
and half-life analysis from proton induced  
spallation and fission reactions of lead and  
uranium  
ICANS-V, Jülich 1981
- /5/ G. Erdtmann, W. Soyka  
The gamma-rays of the radionuclides  
Verlag Chemie, Weinheim and New York 1979

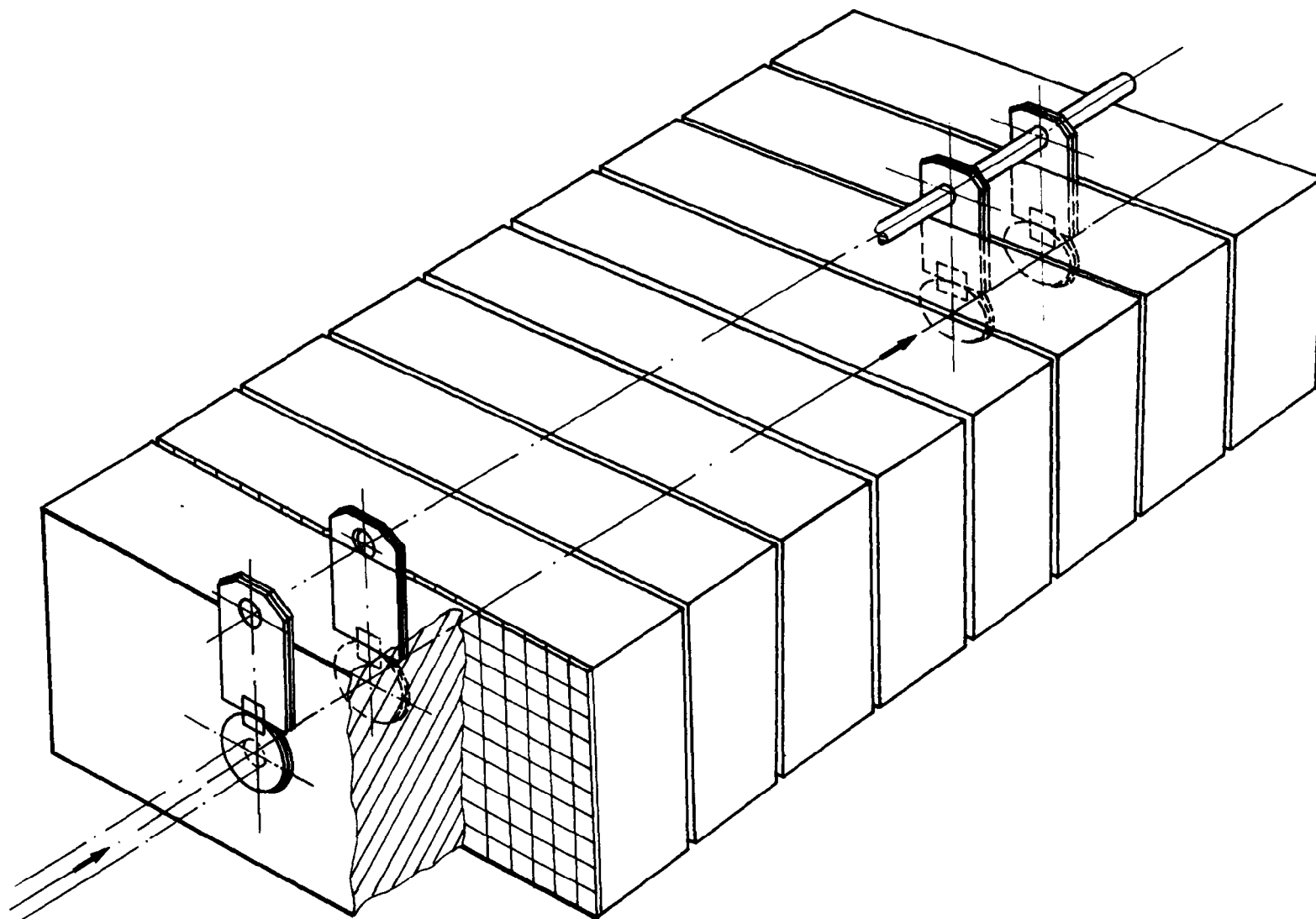
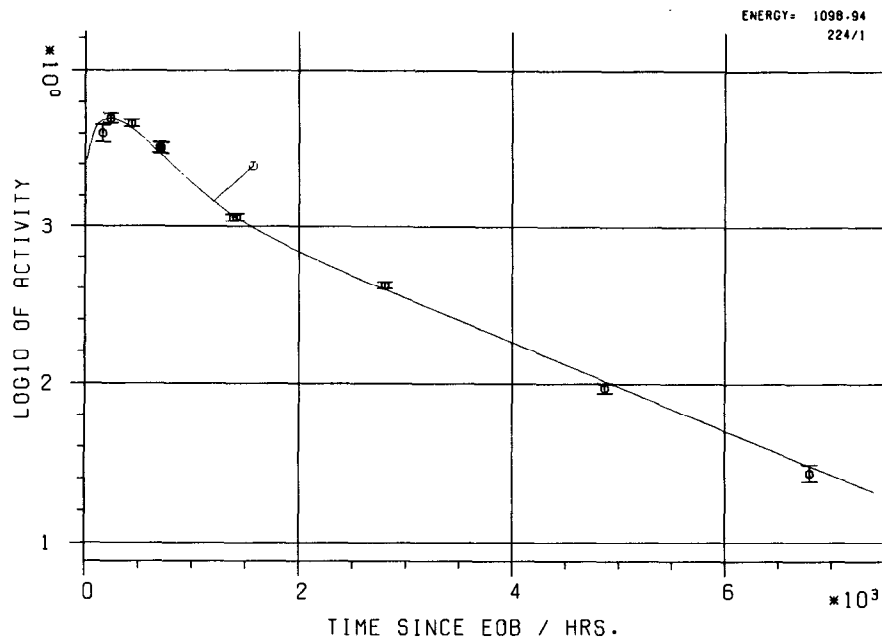


Fig. 1: Target configuration showing the small target disk followed by an aluminum disk and an aluminum plate along with the 5 cm thick Pb brick.



PT 188 --> 10.30 D AD= 9.49E+03-- 3.37E+00  
 --> 77 IR 188 --> 1.73 D AD= 1.52E+01-- 1.61E+04 CHI= 1.50E+02  
 PO 206 --> 8.83 D AD= 1.47E+04-- 8.53E+01  
 --> 83 BI 206 --> 6.24 D AD= 1.95E+02-- 7.10E+04 CHI= 1.15E+02

ENERGY	ERROR	CORR	LIVETIME	% RESIDUE	CPS ERROR	CTS/S	ENERGY	FWHM	EFFICIENCY	DTICORR
1098.94	0.62	1.051E+00								
10	S-EOB									
72U1 7530	1.593E+02	5.820E+02	4.834E+00	5.02E+02	3.991E+03	1098.37	2.723E+00	5.865E-04	1.080E+00	
72U1 7558	2.334E+02	1.508E+03	2.596E+00	3.510E+02	4.981E+03	1098.58	2.588E+00	5.865E-04	1.050E+00	
72U1 7589	4.289E+02	4.622E+03	2.489E+00	2.482E+02	4.537E+03	1098.76	2.688E+00	5.865E-04	1.022E+00	
72U1 7636	6.954E+02	8.364E+03	1.797E+00	2.445E+02	3.260E+03	1098.62	3.190E+00	5.865E-04	1.011E+00	
72U1 7640	7.089E+02	8.551E+03	1.831E+00	2.715E+02	3.244E+03	1098.66	3.111E+00	5.865E-04	1.011E+00	
72U1 7698	1.383E+03	1.928E+04	2.595E+00	6.219E+01	1.149E+03	1099.30	2.604E+00	5.865E-04	1.004E+00	
72U1 7702	1.415E+03	1.984E+04	2.571E+00	6.150E+01	1.158E+03	1099.24	2.621E+00	5.865E-04	1.004E+00	
72U1 7767	2.806E+03	3.351E+04	1.786E+00	2.203E+01	4.200E+02	1099.19	2.682E+00	5.865E-04	1.002E+00	
72U1 7819	4.868E+03	6.398E+04	1.046E+01	6.765E+00	9.430E+01	1099.36	2.709E+00	5.865E-04	1.000E+00	
72U1 7855	6.798E+03	8.640E+04	4.165E+00	3.385E+00	2.726E+01	1099.34	2.378E+00	5.865E-04	1.000E+00	

ENERGY	ERROR	CORR	HALFLIFE	HLF/H	AD (E-ED)/N	DECAY	I/10	PEAK NR	LINE	INTENS
1098.94	224		4.51E+01 D	1.08E+03	3.56E+03	1.11E+00	1.29E-02	1.00E+00	1098.94 224	1099.22 5.65E+01A
E1Z1	26 FE 59				2.28E+02				1291.47 249	1291.58 4.32E+01A
E4Z3	38 SR 83	1.35E+00 D	3.24E+01	6.36E+18	9.08E-01	6.91E-64	6.58E-01	511.61 99	511.00	5.40E+01A

ENERGY	ERROR	CORR	HALFLIFE	HLF/H	AD (E-ED)/N	DECAY	I/10	PEAK NR	LINE	INTENS
E4Z3	38 SR 83	1.35E+00 D	3.24E+01	6.36E+18	9.08E-01	6.91E-64	6.58E-01	511.61 99	511.00	5.40E+01A
E3Z2	77 IR 188	1.73E+00 D	2.47E+02	9.49E+03	7.56E-01	5.27E-09	6.88E-01	154.44 14	155.03	3.34E+01A

ENERGY	ERROR	CORR	HALFLIFE	HLF/H	AD (E-ED)/N	DECAY	I/10	PEAK NR	LINE	INTENS
E2Z1	83 BI 206	6.24E+00 D	2.12E+02	1.47E+04	9.39E-01	2.21E-10	9.94E-01	803.39 162	803.05	1.00E+02A

ENERGY	ERROR	CORR	HALFLIFE	HLF/H	AD (E-ED)/N	DECAY	I/10	PEAK NR	LINE	INTENS
E2Z1	83 BI 206	6.24E+00 D	2.12E+02	1.47E+04	9.39E-01	2.21E-10	9.94E-01	803.39 162	803.05	1.00E+02A
E3Z2	77 IR 188	1.73E+00 D	2.47E+02	9.49E+03	7.56E-01	5.27E-09	6.88E-01	154.44 14	155.03	3.34E+01A

PO 206 --> 8.83 D AD= 6.86E+03-- 1.14E+02  
 --> 83 BI 206 --> 6.24 D AD= 3.91E+03-- 5.51E+02  
 AND 26 FE 59 1.08E+03 H AD= 2.38E+03-- 6.64E+01 CHI= 1.71E+00  
 PT 188 --> 10.30 D AD= 5.65E+03-- 2.54E+02  
 --> 77 IR 188 --> 1.73 D AD= 1.17E+02-- 4.31E+02  
 AND 26 FE 59 1.08E+03 H AD= 2.46E+03-- 6.91E+01 CHI= 7.38E+00  
 38 SR 83 3.24E+01 H AD= 6.86E+04-- 1.18E+04  
 AND 26 FE 59 1.08E+03 H AD= 2.89E+03-- 1.78E+02 CHI= 2.92E+01

Fig. 2: Decay plot and typical output information of YELLOW

```

-----
40 ZR 95      6.440E+01 D 5.564E+06 SEC 1.546E+03 H
DAUGHTERS: NB 95MNB 95
GENESE: NFI 6.500 NTH ZR 94 NFA MD 98
PARENT1:      0.000E+00
PARENT2:      0.000E+00
 4 LINES
-----
724.18 44.2000A E1;Z0;D0;->E1<- 724.31 7.61E+11 3.85E+10 0.00E+00 0.00E+00 6.07E-01 143 0
756.72 54.8000A E1;Z0;D0;->E1<- 756.85 7.56E+11 3.67E+10 0.00E+00 0.00E+00 1.44E+00 150 0
1 LINES MISSING WITH TOTAL INTENSITY OF 0.0200
-----
#
#
44 RU 103     3.935E+01 D 3.400E+06 SEC 9.444E+02 H
DAUGHTERS: RH103M
GENESE: NTH RU102 NFI 3.090 NFA RH103
PARENT1:      0.000E+00
PARENT2:      0.000E+00
23 LINES
-----
294.98 0.2420A EB;Z1;D0;->Z1<- 294.36 1.01E+12 2.23E+11 0.00E+00 0.00E+00 1.57E+00 51 0
317.72 -1.0000A
443.80 0.3110A E5;Z#;D0;->Z#<- 444.70 1.88E+12 1.74E+11 0.00E+00 0.00E+00 8.63E+00 87 0
497.08 86.4000A E1;Z0;D0;->E1<- 497.25 1.03E+12 5.37E+10 0.00E+00 0.00E+00 8.35E-01 98 0
557.04 0.7600A E1;Z4;D0;->Z4<- 557.65 1.11E+12 7.84E+10 0.00E+00 0.00E+00 1.72E+00 110 0
610.33 5.3000A E1;Z0;D0;->E1<- 610.55 9.98E+11 5.66E+10 0.00E+00 0.00E+00 1.36E+00 119 0
13 LINES MISSING WITH TOTAL INTENSITY OF 0.1790
-----
#
#
57 LA 140     4.027E+01 H 1.105E+06 SEC 3.070E+02 H
DAUGHTERS:
GENESE: NFI 6.300 NTH LA139 NFA CE140
PARENT1: BA 140 1.279E+01 D
PARENT2:      0.000E+00
41 LINES
-----
131.12 0.5300A E#;Z0;D0;->E#<- 129.57 1.83E+15 3.19E+14 0.00E+00 0.00E+00 8.41E+02 7 0
241.96 0.4200A E2;Z0;D0;->E2<- 242.22 4.99E+11 1.54E+11 0.00E+00 0.00E+00 2.05E-01 38 0
266.55 0.5200A E4;Z#;D0;->Z#<- 267.64 2.28E+06 7.38E+08 1.68E+07 2.74E+09 5.62E+00 45 1
328.75 18.5000A E1;Z0;D0;->E1<- 329.02 6.68E+07 1.26E+11 5.28E+11 3.28E+09 5.13E+00 61 1
432.55 2.9800A E1;Z1;D0;->Z1<- 432.80 5.48E+04 2.23E+07 5.09E+11 1.04E+08 1.01E+00 84 1
487.03 43.0000A E1;Z1;D0;->Z1<- 487.45 2.35E+08 3.47E+09 5.12E+11 7.17E+09 1.13E+00 96 1
510.95 0.3500A E6;Z#;D0;->Z#<- 511.61 4.95E+13 2.35E+12 2.99E+13 1.52E+12 3.86E+00 99 1
574.20 -1.0000A
751.79 4.1900A E1;Z0;D0;->E1<- 751.81 1.54E+07 1.27E+11 5.25E+11 3.51E+09 6.36E+00 149 1
815.80 22.3200A E1;Z1;D0;->Z1<- 816.21 2.96E+06 3.08E+08 5.23E+11 8.22E+08 8.29E+00 167 1
867.86 5.3600A E1;Z1;D0;->Z1<- 868.02 7.62E+04 1.34E+08 4.99E+11 6.02E+08 1.65E-01 178 1
919.60 2.6100A E1;Z1;D0;->Z1<- 919.57 2.82E+05 3.57E+06 4.97E+11 1.67E+07 2.52E+00 192 1
925.25 6.9200A E1;Z3;D0;->Z3<- 925.52 3.16E+08 1.40E+09 4.96E+11 2.98E+09 2.66E+00 194 1
951.02 0.4900A E3;Z6;D0;->Z6<- 951.95 1.65E+06 3.20E+09 4.10E+09 1.50E+10 6.25E+00 199 1
1085.20 -1.0000A
1596.20 95.4700A E1;Z1;D0;->Z1<- 1596.61 1.37E+04 1.58E+09 5.15E+11 7.42E+09 2.64E-01 282 1
16 LINES MISSING WITH TOTAL INTENSITY OF 0.4300
-----
#
#
#

```

Fig. 3: List of candidate nuclides

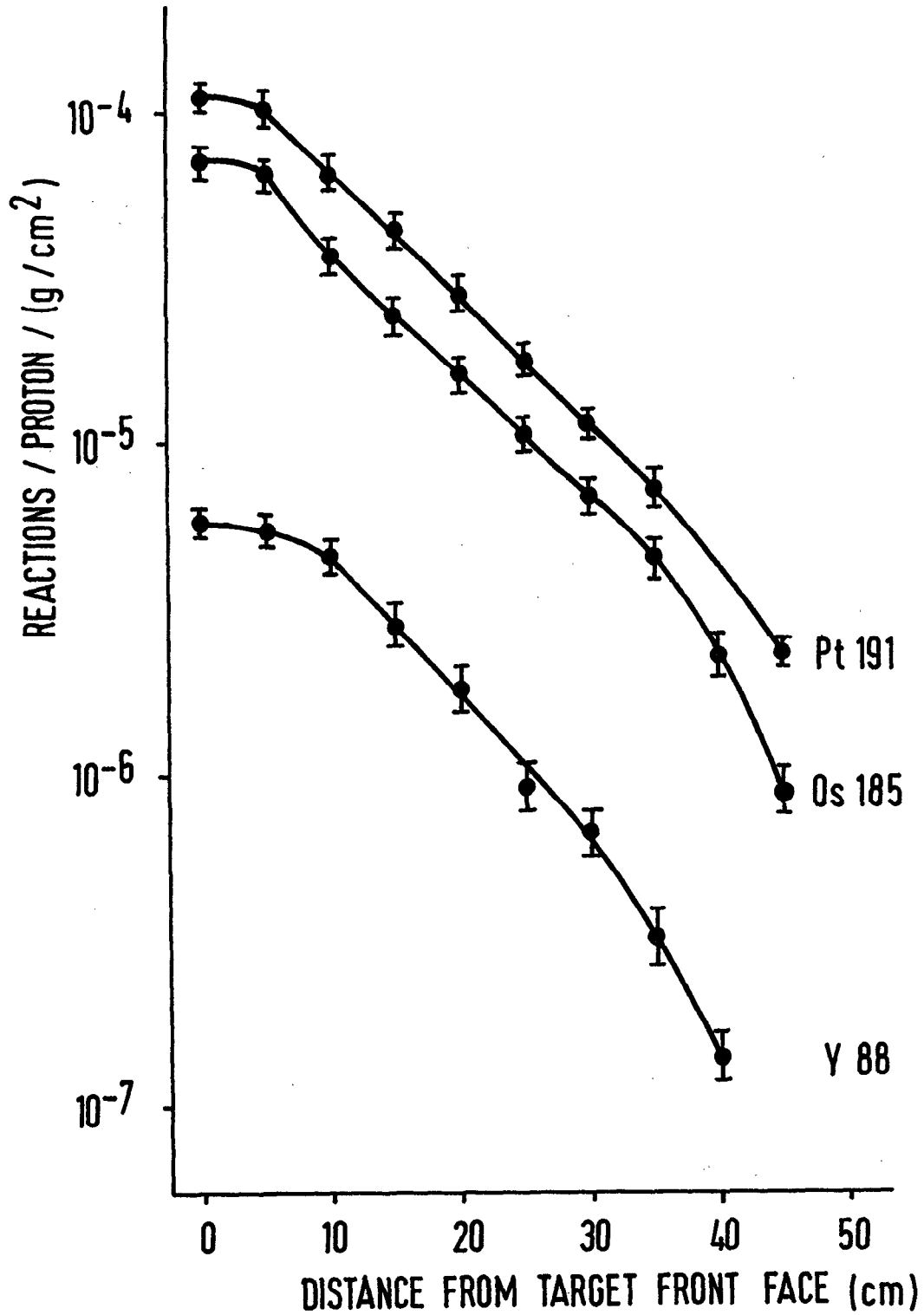


Fig. 4: Axial distributions of Pt191, Os185 and Y88  
within an 1.5 cm radial interval around beam axis

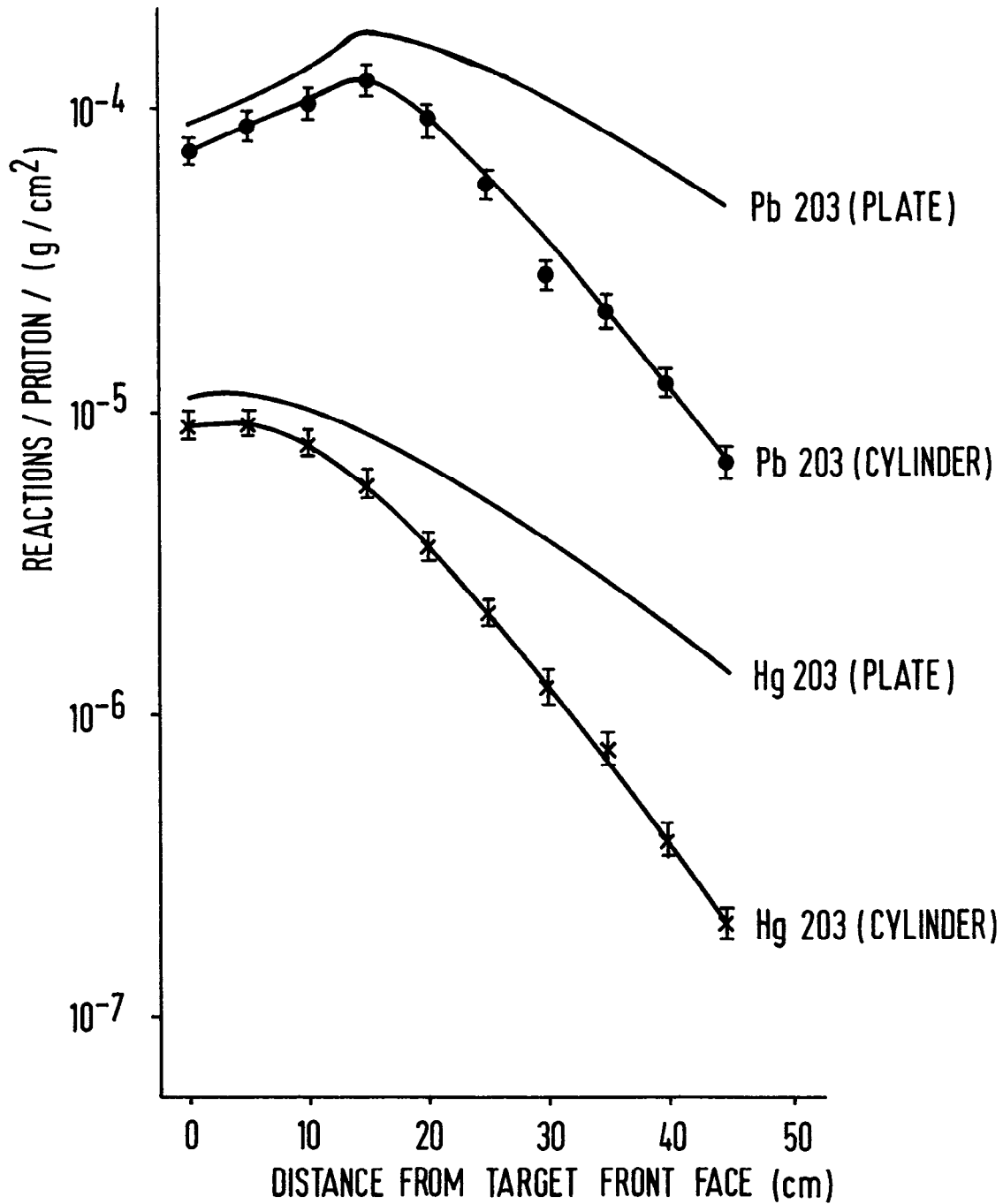


Fig. 5: Axial distributions of Pb<sup>203</sup> and Hg<sup>203</sup> within an 15 mm diameter cylinder around beam axis and within an 100 x 50 x 1 mm plate

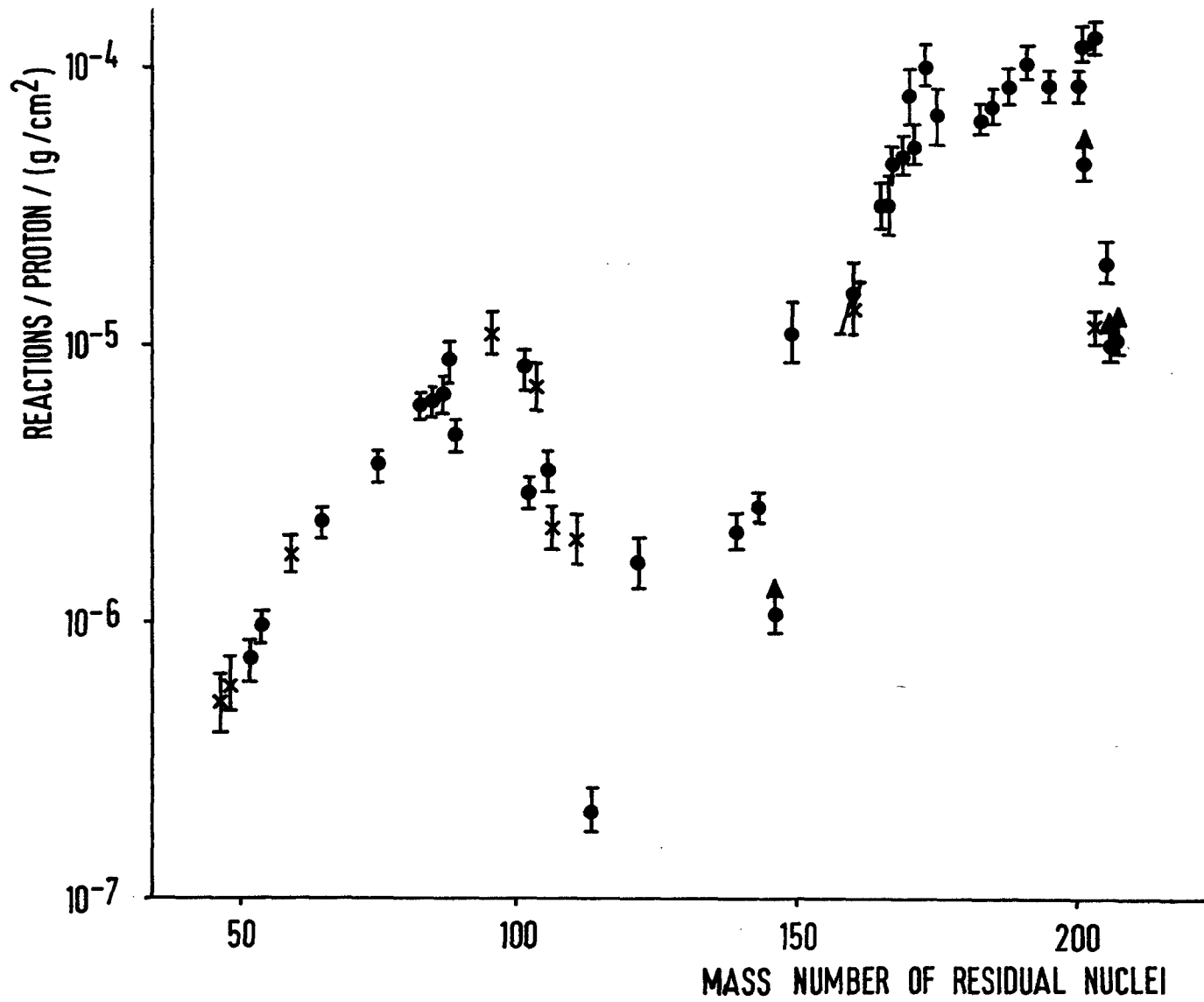


Fig. 6: Mass yield distribution for natural lead at target front face at 1100 MeV ( $\bullet$   $\beta^+$ ,  $\epsilon$ ; X  $\beta^-$ )

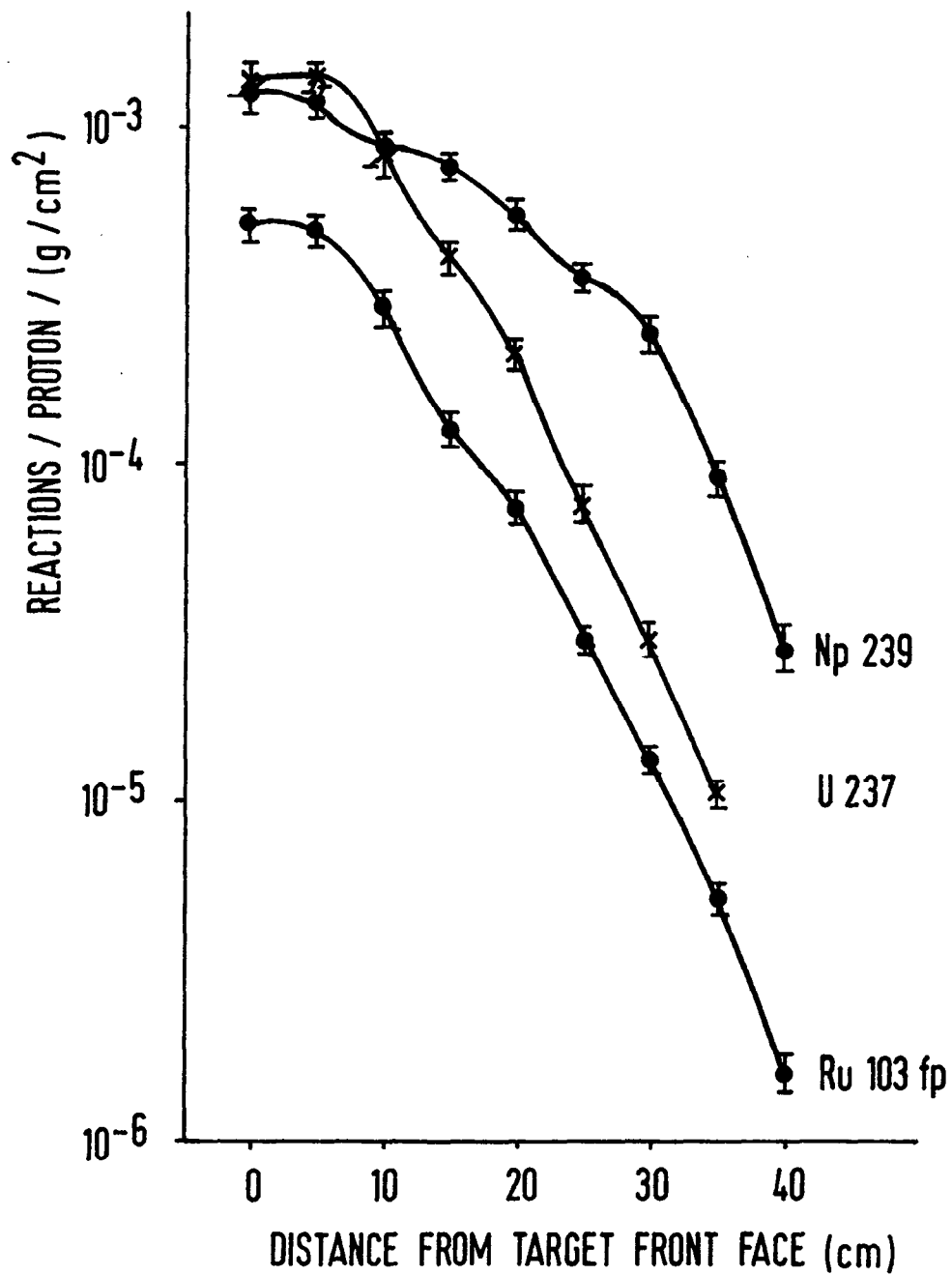


Fig. 7: Axial distributions of Np239, U237 and Ru103 within an 1.5 cm radial interval around beam axis. The distribution of fissions is  $\sim 20$  times that of Ru103 (uranium, 1100 MeV)



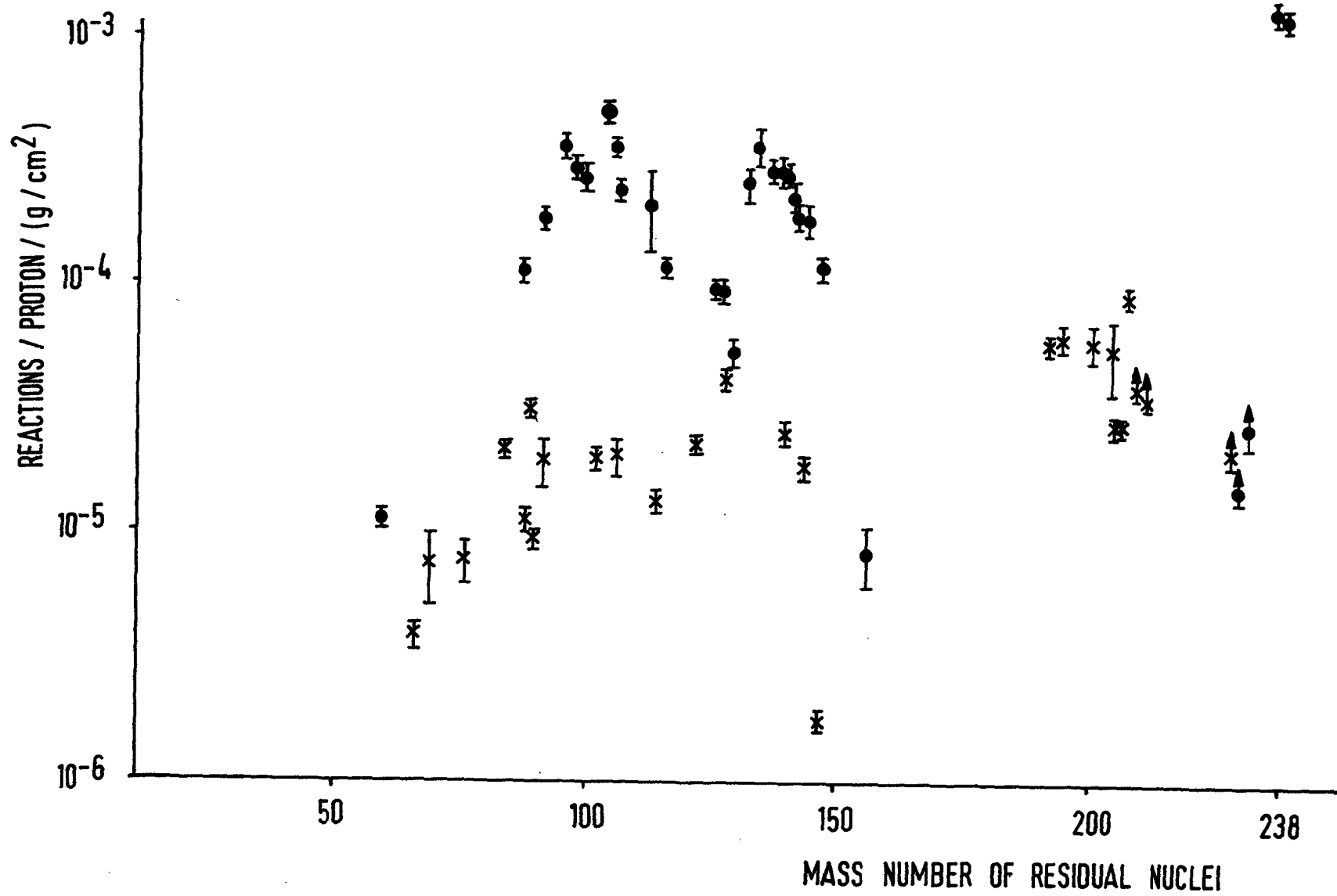


Fig. 8: Mass yield distribution for depleted uranium at target front face at 1100 MeV ( $\bullet$   $\beta^-$ ; X  $\beta^+$ ,  $\epsilon$ )

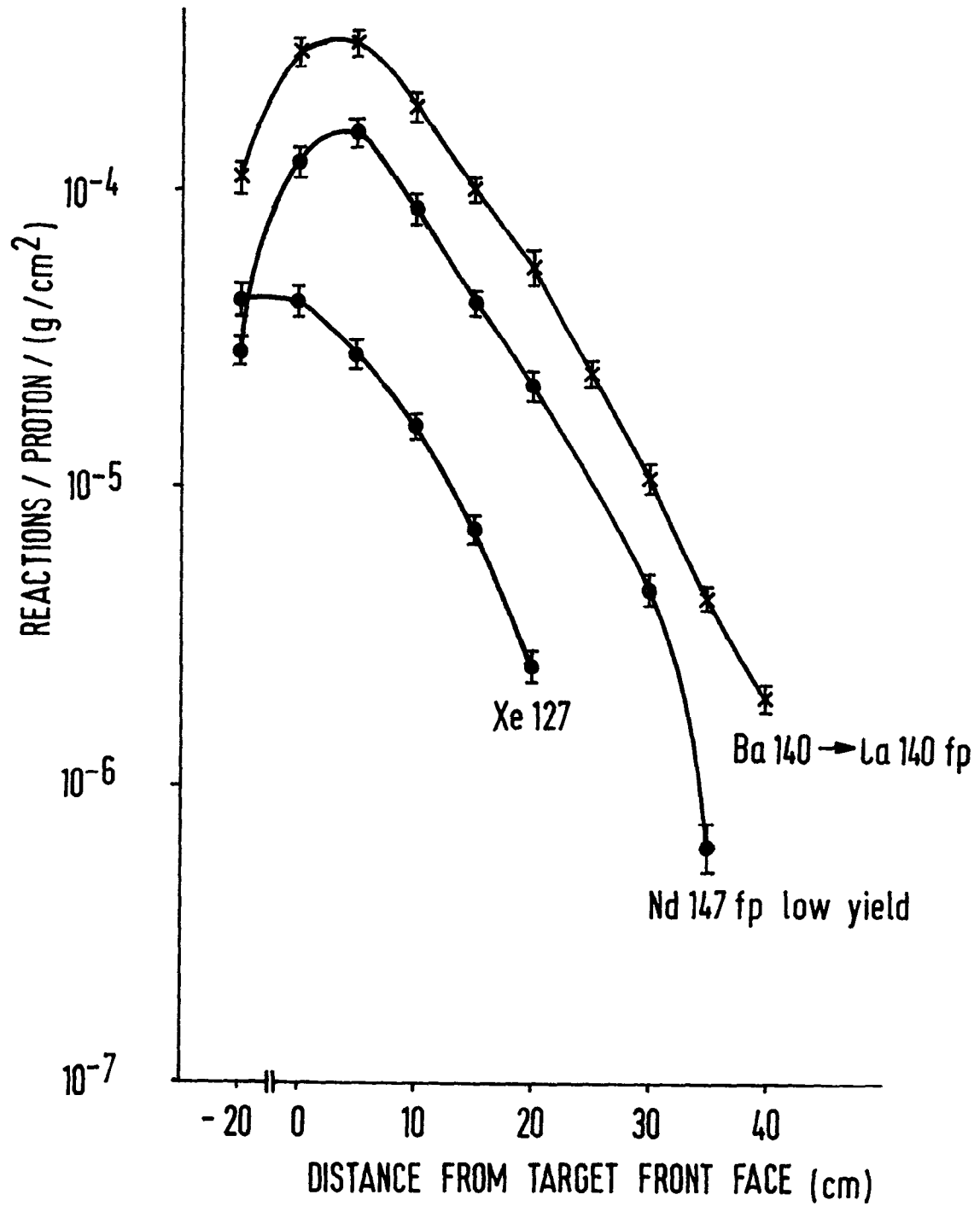


Fig. 9: Axial distributions of Ba140, Nd147, Xe127 compared to thin foil results 20 cm in front of the target (uranium, 1100 MeV)

Reaction	Cross Section (mb)
$^{27}\text{Al}(p,x)^{24}\text{Na}$	11
$^{27}\text{Al}(p,x)^{22}\text{Na}$	12
$^{27}\text{Al}(p,x)^7\text{Be}$	8

Table 1: Al monitor foil data for 1100 MeV protons

Target	Depth (cm)	$\mu_{\text{vert}}$ (cm)	FWHM ( $\Gamma$ cm)	Intensity (c/sec)	% on Target
1	0	-1.24	1.3	255	81
2	5	-1.13	1.8	230	80
3	10	-1.06	2.4	172	76
4	15	- .97	3.2	100	67
5	20	- .89	4.3	58	56
6	25	- .80	5.8	33	45
7	30	- .73	7.9	19	34
8	35	- .62	10.6	11	28
9	40	- .54	14.4	6.2	19
10	45	- .46	19.4	4.6	15

( $\mu_{\text{horiz}}$  = + .095 cm)

Table 2: Beam Parameters from  $^{24}\text{Na}$  Measurements for the

Nuclide	Halflife	Activity at Saturation* (MBq/nA)
Hg 203	46.6 d	20
Pb 203	52.1 h	380
Tl 201	73.5 h	220
Pt 191	2.8 d	190
Os 185	94.0 d	110
Re 183	71.0 d	120
Zr 95	64.0 d	20
Y 88	108.0 d	11

\*numbers estimated to be correct within a factor of two

Estimated activities at saturation for some dominant  
 $\alpha$ -emitters

Nuclide	Halflife	Activity at Saturation (MBq/nA)
Pt 190	$6.1 \cdot 10^{11} \text{ a}$	180
Os 186	$2.0 \cdot 10^{15} \text{ a}$	140
Hf 174	$2.0 \cdot 10^{15} \text{ a}$	130

Table 3: Activity at saturation per nA proton current of 1100 MeV within a 45 cm long, 10 cm \* 5 cm area lead target